Journal Pre-proof



What constitutes woody cover? Physiognomic-structural characterizations vary between woody cover maps in dryland ecosystems

Xinyuan Li, Matthew Hansen, Peter Potapov, Alexandra Tyukavina, Cheikh Mbow, Amadou Moctar Dieye, Abdoul Aziz Diouf, Andrew Poulson, Andres Hernandez-Serna, Jeffrey Pickering, Babacar Ndao, Cheikh Mame Mor Mbodji, Katherine Melocik

PII: S2666-0172(26)00171-9

DOI: https://doi.org/10.1016/j.srs.2026.100533

Reference: SRS 100533

To appear in: *Science of Remote Sensing*

Received Date: 6 July 2026

Revised Date: 27 September 2026

Accepted Date: 27 October 2026

Please cite this article as: Li, X., Hansen, M., Potapov, P., Tyukavina, A., Mbow, C., Dieye, A.M., Diouf, A.A., Poulson, A., Hernandez-Serna, A., Pickering, J., Ndao, B., Mbodji, C.M.M., Melocik, K., What constitutes woody cover? Physiognomic-structural characterizations vary between woody cover maps in dryland ecosystems, *Science of Remote Sensing*, https://doi.org/10.1016/j.srs.2026.100533.

This is a PDF of an article that has undergone enhancements after acceptance, such as the addition of a cover page and metadata, and formatting for readability. This version will undergo additional copyediting, typesetting and review before it is published in its final form. As such, this version is no longer the Accepted Manuscript, but it is not yet the definitive Version of Record; we are providing this early version to give early visibility of the article. Please note that Elsevier's sharing policy for the Published Journal Article applies to this version, see: https://www.elsevier.com/about/policies-and-standards/sharing#4-published-journal-article. Please also note that, during the production process, errors may be discovered which could affect the content, and all legal disclaimers that apply to the journal pertain.

© 2026 Published by Elsevier B.V.

Journal Pre-proof

What constitutes woody cover? Physiognomic-structural characterizations vary between woody cover maps in dryland ecosystems

Xinyuan Li[a*], Matthew Hansen[a], Peter Potapov[b], Alexandra Tyukavina[a], Cheikh Mbow[c], Amadou Moctar Dieye[c], Abdoul Aziz Diouf[c], Andrew Poulson[a], Andres Hernandez-Serna[a], Jeffrey Pickering[a], Babacar Ndao[c], Cheikh Mame Mor Mbodji[c], Katherine Melocik[d]

[*]Correspondence to: Xinyuan Li (lxy95@umd.edu)

Affiliations

[a]Department of Geographical Sciences, University of Maryland, College Park, MD, USA
[b]World Resources Institute, Washington, D.C., USA
[c]Centre de Suivi Ecologique, Dakar, Senegal
[d]NASA Goddard Space Flight Center, Greenbelt, MD, USA

Keywords

Drylands, woody cover map, height, physiognomic structural trait, unoccupied aerial vehicles (UAV), Lidar

Abstract

Dryland ecotones are challenging to map, but technical advances promise improved characterization of woody cover and associated ecosystem services. However, definitions of woody cover are often vague or lacking physiognomic-structural thresholds, limiting the understanding of map quality. Using unoccupied aerial vehicle (UAV) lidar data, we show that continental-scale maps using advanced data and algorithms have low spatial agreement and correspond to different physiognomic-structural thresholds over Senegal. The woody cover area where all examined maps agree accounts for only 2.8% of the country. Each map differs in its best-matching structural definition, with height thresholds ranging from >2 m to >6 m and cover thresholds from >34% to >55%; the resulting F-1 ranged from 0.24 to 0.63. Although based on a non-probability sample, the results illustrate the need for robust practices in defining and validating dryland woody cover map characterizations. Without such harmonization, it will remain challenging to conduct higher level analyses (e.g. carbon accounting, ecosystem monitoring or habitat assessments) and decision-making that requires accurate maps. Through this brief communication, we call for the harmonized use of physiognomic structural traits for building definitions in dryland woody cover mapping.

Science for Society

Dryland woody cover plays a critical role in maintaining ecosystem stability and supporting human livelihoods, particularly in developing regions. Accurate, spatially explicit satellite maps of woody cover are essential for informing land management and environmental sustainability policies. However, using high-resolution UAV lidar data across Senegal, we show that the state-of-the-art deep learning-based large-scale maps exhibit substantial spatial and structural disagreements in mapped woody cover. This lack of convergence stems from ambiguous definitions of woody cover, undermining map usage in science and policy. Without harmonizing the use of physiognomic-structural traits (height and cover) in defining woody cover, map accuracy cannot be validated or compared. Establishing such harmonization is essential for robust carbon accounting, ecosystem monitoring, and land management in drylands worldwide.

Main Text

1. Introduction

Dryland woody cover provides irreplaceable services in regulating ecosystems and supporting local livelihoods (Pan et al., 2011; Brandt et al., 2018). Over the last century, it has undergone extensive changes driven by complicated mechanisms - the loss from both human-induced and natural degradation; and the gain from the "greening trend" due to the changing climate and restoration efforts (Brandt et al., 2018; Venter et al., 2018). Large-scale remote sensing-based maps have been generated to support policies aimed at improving livelihoods and sustaining environments associated with woody cover (Brandt et al., 2020; Brandt et al., 2023; Reiner et al., 2023). However, our analysis shows that convergence of dryland woody cover estimates is not yet realized.

Before the earth observation era, Küchler (1949) pointed out that "scientific comparisons of widely separated areas" were challenging as methods for mapping vegetation precluded a "comparative approach." Townshend et al. (1991), in establishing the discipline of large area mapping using remotely sensed imagery (Defries and Townshend, 1994; Tucker, 1979), emphasized the solution to this limitation through the consistent observational coverage and algorithmic characterization of satellite time-series data. However, this assumption is not a given. A key source of variance in earth observation-derived maps is the inconsistent application of data and/or algorithms to nominally the same target. Legends defining the classes of interest are often ambiguous or not consistently treated across different methodological approaches. These challenges are particularly acute for drylands, where woody cover life forms vary greatly in size and distribution. Unlike a uniform closed canopy forest class (e.g., >80% canopy cover and >10m height), dryland ecotones feature shorter, less dense distributions that are harder to discriminate. Without clear thresholds defining the structural limits of woody cover type(s), it remains difficult to consistently validate the accuracy and corresponding reliability and usability of a woody cover map.

The Land Cover Meta Language (LCML) (ISO 19144-2:2023, 2023), succeeding the United Nations Food and Agriculture Organization's (FAO) Land Cover Classification System (LCCS) (Di Gregorio et al., 2016), provides a detailed conceptual and operational framework for applying classifiers in building legends for mapping land cover, including growth form, height, cover, spatial distribution, minimum mapping unit and other attributes. Per White (1983), Pratt et al. (1966) and others, physiognomic structural traits, such as height and cover can be used to define categories of woody cover (Fig. 1). These two traits have also been used by a number of global classification schemes to define the extent of woody cover (FAO, 2023; Hansen et al., 2000; IGBP, 1992; Loveland et al., 2000). The Intergovernmental Panel on Climate Change (IPCC) leaves countries and institutions free to apply different forest definitions with a range of height and cover alternatives (UNFCCC, 2001). In recent years, the use of high (~10 m; e.g., Sentinel-2) and very high (~0.5 m ~ 3 m; e.g., DigitalGlobe and PlanetScope) spatial resolution imagery has advanced the mapping of dryland woody cover to identify individual trees and shrubs using deep learning algorithms (Brandt et al., 2020; Brandt et al., 2023; Reiner et al., 2023). However, these maps either do not provide definitive height/cover thresholds of the mapped target (Brandt et al., 2020); or state the physiognomic-structural definitions that are not directly reflected in the reference data used to make the maps (Brandt et al., 2023; Reiner et al., 2023). These limitations reduce comparability among the maps and increase uncertainty in their application.

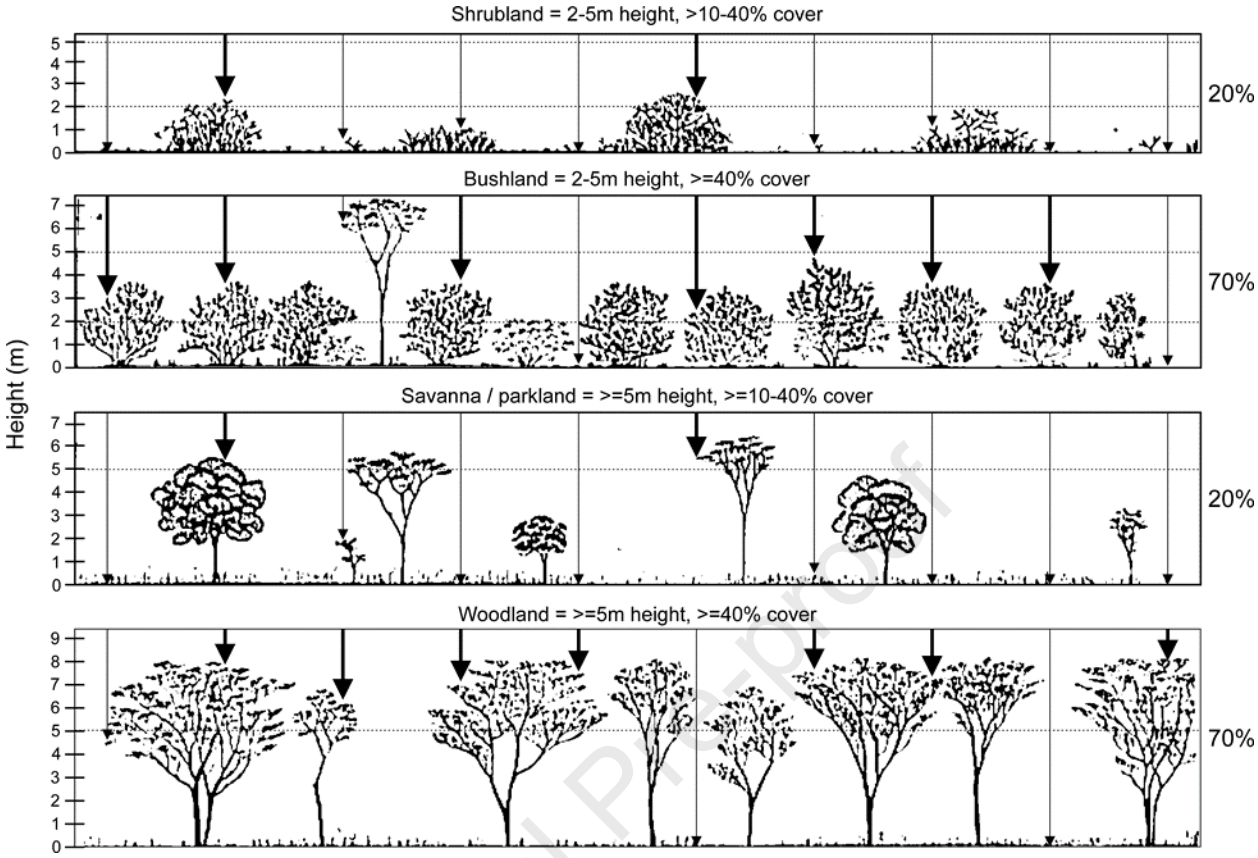


Fig. 1. Example of woody cover classes as defined by height/cover thresholds. Bold arrows indicate skylight orthogonal to the ground that is intercepted by crown extent. Note that 'crown extent cover' here differs from the UAV lidar-derived foliar cover shown in Fig. 3, which refers to the leaf area intercepted by skylight. Figure adapted from Pratt et al. (1966).

Here, we evaluate three of the most advanced large-area woody cover maps (Table 1) over Senegal (Brandt et al., 2020; Brandt et al., 2023; Reiner et al., 2023). The agreement of the mapped targets is quantified and assessed in terms of their physiognomic structure using fine-scale field-based unoccupied aerial vehicle (UAV) lidar (light detection and ranging)-derived vegetation height/cover information (S1). The primary outcome is an intercomparison of three large area maps for the country of Senegal, chosen as an accessible dryland ecotone from Sudanian woodlands to Sahelian shrubland and steppes. The lidar data, though not a probability sample, covers the dominant range of woody height and cover across the ecotone (Fig. 2).

2. Study Area

Senegal consists of four ecoregions (White, 1983; Dinerstein et al., 2017; Fig. 2). The West Sudanian savanna (58.2%) is within the Sudanian regional center phytochorion, which is rich in endemic species and consists of a vegetation gradient from grasses to shrubs to woodland from north to south. The Sahelian Acacia savanna (27.6%) is within the Sahel regional transition zone, bordering the Sahara regional transition zone to the north, and featuring grass-dominated land with scattered shrubs and trees on sandy soils. Vegetation height is highly dependent on water accessibility in this region. Guinean forest-savanna mosaic (13.5%) and Guinean mangroves (0.7%) are within the Guinea-Congolia/Sudania regional

transition zone. The former features distributions of savanna and forest, represented by the gallery forest along rivers on the east and big patches of dense tropical forests on the west. The latter features extensive mangrove forests distributed along the coast that support unique biodiversity. The climate gradient and resulting diversity of vegetation forms across Senegal makes it suitable for studies of gradients of vegetation physiognomic- structural traits.

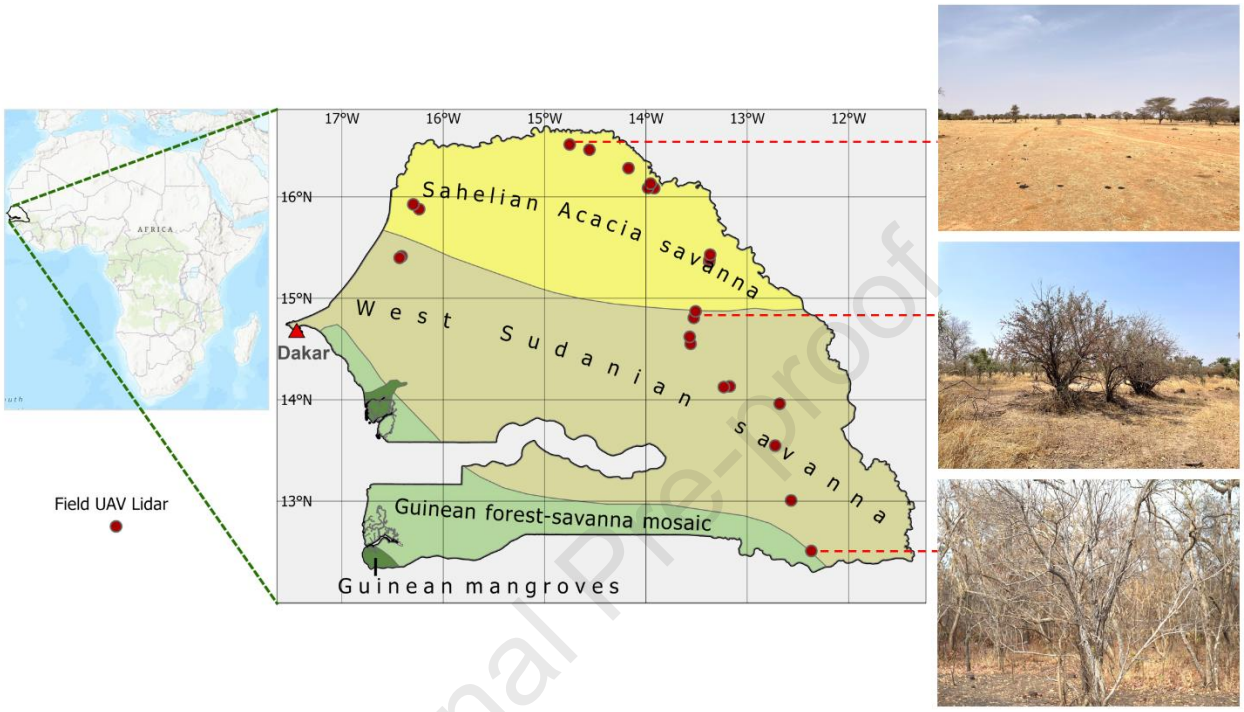


Fig. 2. Ecoregions of Senegal and field study sites where UAV-based data were collected using RIEGL lidar equipment. Ecoregion boundaries are from Dinerstein et al. (2017). The change of the vegetation along the ecological gradient over the country is shown in the field photographs on the right.

3. Datasets

3.1 Existing Woody Cover Maps

We examined three large-area woody cover maps (Table 1), all produced using U-Net, a convolutional neural network-based deep learning architecture (Brandt et al., 2020; Brandt et al., 2023; Reiner et al., 2023). Brandt et al. (2020) used DigitalGlobe imagery to map trees outside of forests. The map is a 0.5 m binary tree crown mask of the woody plants with a crown size >3 m² (no height threshold or other structural parameters employed). In validation, they reported 25% missed tree cover area, and a 2% false positive rate. Reiner et al. (2023) mapped all woody vegetation with heights above 5 to 6 m in Africa using PlanetScope imagery, using the presence of shadow as the criteria for collecting reference data. The map is a 1 m resolution binary tree mask. They specifically reported accuracy for Senegal by comparing percent tree cover aggregated at the plot level between the map and lidar reference across multiple plots. The lidar reference tree cover was derived using a 6 m height threshold applied to a lidar canopy height model (CHM), resulting in an R^2 of 0.81 and RMSE of 16.21%. World Resource Institute (WRI) created a 10 m tropical tree extent map from Sentinel 1&2 imagery, defining trees as woody vegetation that has either height >5 m, or crown size ≥5 m diameter and 3-5 m height (Brandt et al., 2023). During reference data collection, height was estimated through visual inspection and shadow was used as a primary guide. The

WRI map is a 10 m tree extent probability layer representing the "probability of one or more tree canopies intersecting the centroid of a 10 m pixel". The tree extent map was validated at a probability threshold of 35%, with a UA of 96.1%, PA of 97% and OA of 94%.

Source	**Brandt et al. (2023)** (WRI)	**Reiner et al. (2023)**	**Brandt et al. (2020)**
Mapped Target	Tree extent in tropics (-23.44°~23.44° latitude)	Forest and non-forest tree cover in Africa	Non-forest trees in the West African Sahara, Sahel and sub-humid zone
Data Year	2020	2019	2005 - 2018
Resolution	10 m	1 m	0.5 m
Satellite Imageries Used	Sentinel-1 Sentinel-2	PlanetScope	DigitalGlobe
Tree Definition	(Height >5 m) or (3 m ≤ height ≤ 5 m & crown diameter ≥ 5 m)	Height ≥ 5 or 6 m	crown size > 3 m²
Reference Data	WorldView imagery (trees identified by visual interpretation of height/ presence of shadow)	Google Earth imagery & Bing imagery (trees identified as woody plants with shadow)	DigitalGlobe imagery (trees identified by NDVI, shadow and crown size)
Product Delivered	10 m probability map	1 m binary tree/no tree map	0.5 m binary tree crown map

Table 1 The summary of the maps that were compared in this study: Brandt et al. (2020), Brandt et al. (2023) and Reiner et al. (2023).

3.2 UAV-based Lidar Data

UAV-based lidar data provide direct high-density three-dimensional measurements of vegetation structure and have demonstrated performance comparable to terrestrial laser scanning systems (Brede et al., 2017; Reckziegel et al., 2025). Therefore, they provide reliable reference data and were used for map intercomparisons and benchmarking assessments in this study. The data were acquired through a RIEGL miniVUX-SYS (with AP20) laser scanner system mounted over a DJI Matrice 600 Pro platform. The sensor emits the near infrared laser pulses at 100 kHz pulse repetition rate (PRR). The pulse can penetrate the canopy and trigger multiple returns. The 3D point cloud that contains the positional information of the ground objects can be generated by recording the travel time of each return. The lidar UAV was flown at an altitude of ~25 m with speed ~4 m/s, which resulted in ~500 to 4500 pts/m^2 point density depending on the height of the ground object. The data were collected between 02/20/2023 and 02/27/2023 during the dry season of Senegal to take advantage of suitable weather conditions for UAV operations and road accessibility. While leaf conditions of deciduous vegetation during this period may affect lidar observations, woody vegetation structure remains detectable by lidar through stems and branches, and a substantial portion of woody vegetation in Senegal is evergreen (S1). In total, we flew 25 plots. The flight area over each plot adds up to ~132 ha (S1, Fig. 2). Twenty-one plots were collected over natural vegetation along the ecoregional gradient of eastern Senegal, and 4 plots over agroforestry lands on the west coast. The plots

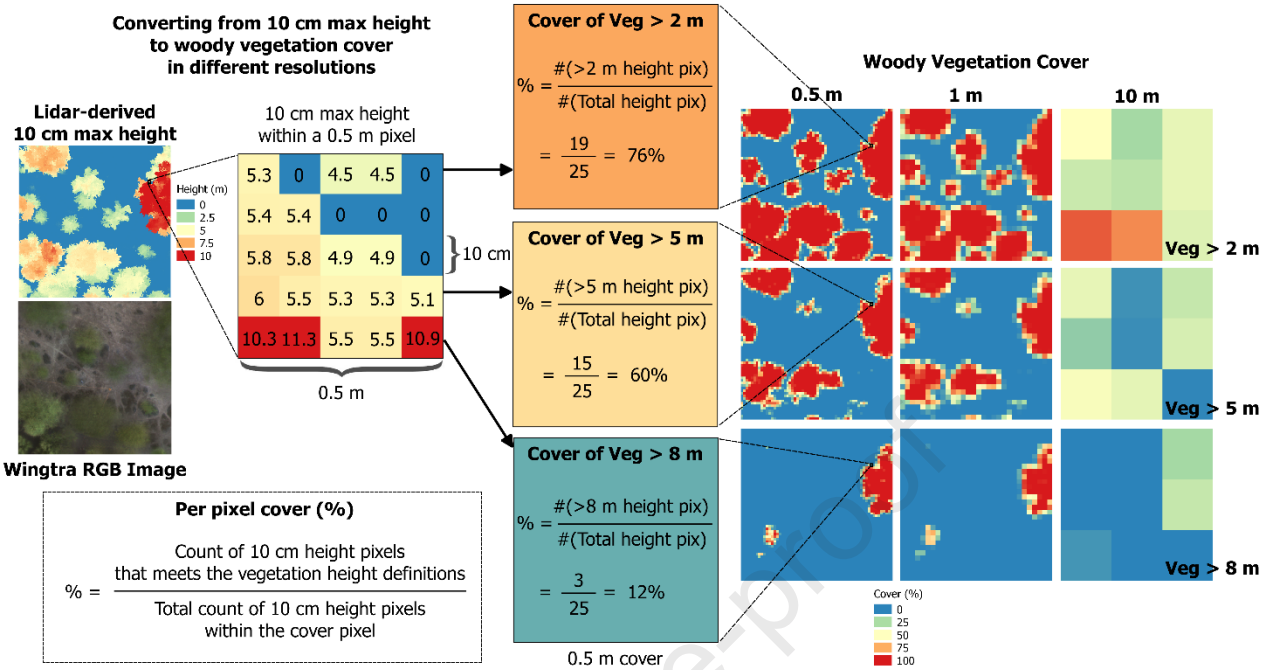
represent a range of vegetation height/cover variation, land uses, soil types and ecoregions. They form essentially a north-south transect across the Sudan-Sahel ecotone of areas absent of near-term disturbance, with added sites within the Senegal River valley and agroforestry zones near the coast.

4. Methods

4.1 Lidar Data Processing

The UAV-based lidar data requires an internal processing, which involves raw data pre-processing using the sensor manufacturer's software, and a subsequent external processing, which uses geospatial software to handle the common data type (LAS 3D point cloud) obtained from internal processing for application purposes. During the internal processing, we first followed a post-processing kinematic (PPK) workflow to calibrate the geolocation of the flight trajectories, using the GPS information obtained from the NovAtel PwrPak7 base station set up during each flight. To do this, the base station log files were first converted to the RINEX format in NovAtel Convert software and then used to obtain National Spatial Reference System (NSRS) coordinates through the Online Positioning User Service (OPUS) provided by NOAA National Geodetic Survey (NGS). The raw flight tracks were then processed using the OPUS solution along with the base station logs in POSPac software to create the calibrated flight tracks with centimeter level geolocation accuracy. Then we used RiPROCESS software to georeference the laser data with track data and export the point cloud in the widely used LAS format for external processing.

During the external processing, we used LASTools to convert the LAS point cloud into gridded cover maps. First, the ground points were identified using the 'lasground' command. Then, the beyond-ground height of each non-ground point was calculated using the 'lasheight' command. We gridded the point cloud in 10 cm resolution using the max height of the pixel to get the rasterized digital surface model (DSM). After visual examination of the gridded image, we assigned 0 value to the abnormally high values that were caused by the power lines, buildings, people and animals. In very rare cases (less than 0.01% of the lidar-derived cover pixels), woody vegetation >1 m was present below power lines, but the impact was negligible. We also partially removed the edge of the image with artifacts due to the less dense laser scanning. Using the resulting very high-resolution DSM, we were able to generate the reference woody vegetation cover maps under different heights threshold (Fig. 3). We created eight sets of reference cover maps, for woody vegetation above 1 m, 2 m, 3 m, 4 m, 5 m, 6 m, 7 m and 8 m, respectively. For each height threshold, we generated reference cover maps at different resolutions (0.5 m, 1 m, 10 m). The per-pixel percent cover was calculated as the ratio of the count of the 10 cm height pixels that meet the woody vegetation height definitions, to the total count of the 10 cm height pixels within the target resolution pixel extent. In this way, the cover here refers to the foliar cover, which is the leaf area intercepted by the vertical skylight. Note that as the resolution of the reference cover map becomes finer, the map contains more 100% and 0% cover values, with fewer mixed pixels with intermediate cover values (Fig. 3). We visually examined Google Earth, PlanetScope and Landsat time-series imagery to verify that the lidar reference data were located in stable woody cover area that had remained unchanged since 2005, ensuring their suitability in comparing maps generated for different temporal periods. All the lidar plot 10 cm height images are shown in S1.



184

185 **Fig. 3.** The workflow of converting UAV-derived 10cm max height maps to reference cover maps for different height
186 thresholds (>1 m to >8 m) in different resolutions (0.5 m, 1 m, 10 m and 30 m). The calculations of single pixel cover
187 for vegetation >2 m, >5 m and >8 m in 0.5 m are shown. Given that the within-crown gaps were accounted during
188 calculation, the derived cover refers to foliar cover, which is the leaf area intercepted by vertical skylight.

189 *4.2 Benchmarking Assessments & Intercomparisons*

190 We compared the existing maps from Brandt et al. (2020), Reiner et al. (2023) and Brandt et al. (2023)
191 with our lidar-based maps to provide an assessment of the actual woody vegetation cover and height these
192 maps represent in dryland ecosystems. The binary tree/tree crown maps from Brandt et al. (2020) and Reiner
193 et al. (2023) were directly compared to lidar reference maps. For Brandt et al. (2023), as the map probability
194 value lacks consistency and cannot be directly linked to tree cover percentages (S2), we converted the WRI
195 probability layer into a binary map for this study by setting the probability threshold at 50% (≥50% - tree
196 cover presence, <50% - tree cover absence). We also tested a 35% probability threshold (≥35% - tree cover
197 presence, <35% - tree cover absence), following Brandt et al. (2023), to derive an alternative binary tree
198 extent map. All three maps were evaluated in their original resolutions.

199 To link the maps to the specific physiognomic-structure thresholds and assess the corresponding
200 agreements, we varied height and cover thresholds of the lidar data resampled to each map's spatial
201 resolution in order to find a best result - one where omission and commission errors were balanced. To do
202 this, first, the map-derived area of the tree cover was calculated for each map product, over the UAV lidar
203 pixels in the corresponding resolution (0.5 m, 1 m and 10 m). Then, the UAV lidar-derived woody
204 vegetation cover area was also calculated at the eight different height thresholds (>1 m to >8 m). The area
205 comparisons were made between each map and the corresponding eight UAV lidar-derived areas, to
206 examine the best-matching height definition of the "tree" in the map. Finally, we investigated which
207 combination of woody vegetation cover and height from the reference UAV lidar data is best represented

by the maps. To do this, under each best-matching height definition, the continuous reference map of UAV lidar-derived percent woody vegetation cover was converted into a set of binary woody cover masks at each 1% cover increment. We then compared the area of those binary masks with the area of the corresponding evaluated binary tree cover map. The confusion matrices were generated for each combination of reference and evaluated binary masks, and map accuracy metrics were computed. Specifically, the user's accuracy (UA) for the woody cover was calculated as the ratio of the count of correctly mapped woody cover pixels to the total mapped woody cover pixels. The producer's accuracy (PA) for the woody cover was calculated as the ratio of the count of correctly mapped woody cover pixels to the total reference woody cover pixels. And the overall accuracy (OA) was calculated as the ratio of the count of correctly mapped pixels to the total validation pixels. The F-1 score for both evaluations were calculated as:

$$F1 = \frac{2 * PA * UA}{PA + UA}$$

Note that the reported accuracy metrics quantify agreement with the lidar-derived physiognomic-structure definitions, rather than the accuracy of each product under its original target definitions. In addition, the geolocation inaccuracies in Brandt et al. (2020) were accounted for in the evaluations. To do this, for each lidar plot, we shifted the Brandt et al. (2020) data around to find a highest correlation with the lidar-based mask. The accuracy metrics and the confusion matrix were then generated based on the comparisons between the georeferenced Brandt et al. (2020) and lidar-derived binary masks.

We also quantified the spatial agreement among the maps. The three maps were overlapped over the whole Senegal and the area proportions of the mismatches and overlaps were calculated. We have also overlapped the lidar reference binary maps with the three maps over the lidar flight area under the most inclusive best-matching definitions (Brandt et al. (2023) >2 m height, >34% cover). The comparisons were performed at the 0.5 m scale. Reiner et al. (2023) and Brandt et al. (2023) maps were resampled to 0.5 m for intercomparisons. Meanwhile, aggregating each map to a coarser level cover (e.g. 10 m) for comparisons will help reduce the spatial heterogeneity originating from the scale differences of each source. We did this by calculating and adding up the per-pixel percent cover agreements/disagreements under the assumption that the mapped tree/woody cover in each pixel co-located among different sources. Specifically, Reiner et al. (2023) 1 m and Brandt et al. (2020) 0.5 m binary maps were aggregated to the 10 m percent cover maps and the 10 m probability value of Brandt et al. (2023) was used directly.

In addition, to obtain a spatial overview for visualization purposes, we generated a 30 m RGB composite by aggregating maps of Brandt et al. (2020), Reiner et al. (2023) and Brandt et al. (2023) into 30 m resolution and placing the aggregated maps into red, green and blue channels of the composite, respectively. The overlaps and mismatches among different maps can be then highlighted in different colors in the composite. For the Brandt et al. (2023), the 30 m cover map was generated by taking the mean of the 10 m probability within each 30 m pixel. For both Reiner et al. (2023) and Brandt et al. (2020), the 30 m cover maps were calculated by dividing the count of tree pixels by the total count of 1 m and 0.5 m pixels, respectively, within each 30 m pixel.

5. Results

When looking at the spatial agreement among different maps (Fig. 4), only Brandt et al. (2020) captures small crowns over the middle Sudanian region (dark red) while it disagrees with the other maps (cyan) over dense canopy in the south and is also subject to data artifacts and inconsistencies that affect map quality.

Reiner et al. (2023) captures the least tree cover (magenta) and suffers from patchy artifacts (green). Conversely, Brandt et al. (2023) has the most tree cover (wide-spread magenta and cyan) except for within the middle Sudanian zone, and overall has fewer artifacts and discontinuities. Quantitatively, each map differs in tree cover proportion estimates with the number ranging from 10.8% to 29.2% over the whole Senegal (Fig. 5(a)). A total of 35.8% of the country was mapped as tree cover by at least one of the three maps and this number is more than three times the area mapped by Reiner et al. (2023) and nearly three times that of Brandt et al. (2020). The woody cover area where all three maps agree accounts for only 2.8% of the country. The disagreement among different maps highlights inconsistencies in defining woody cover and emphasizes the importance of applying consistent physiognomic-structural definitions for short, sparse woody ecotones in facilitating intercomparisons and assessing accuracy.

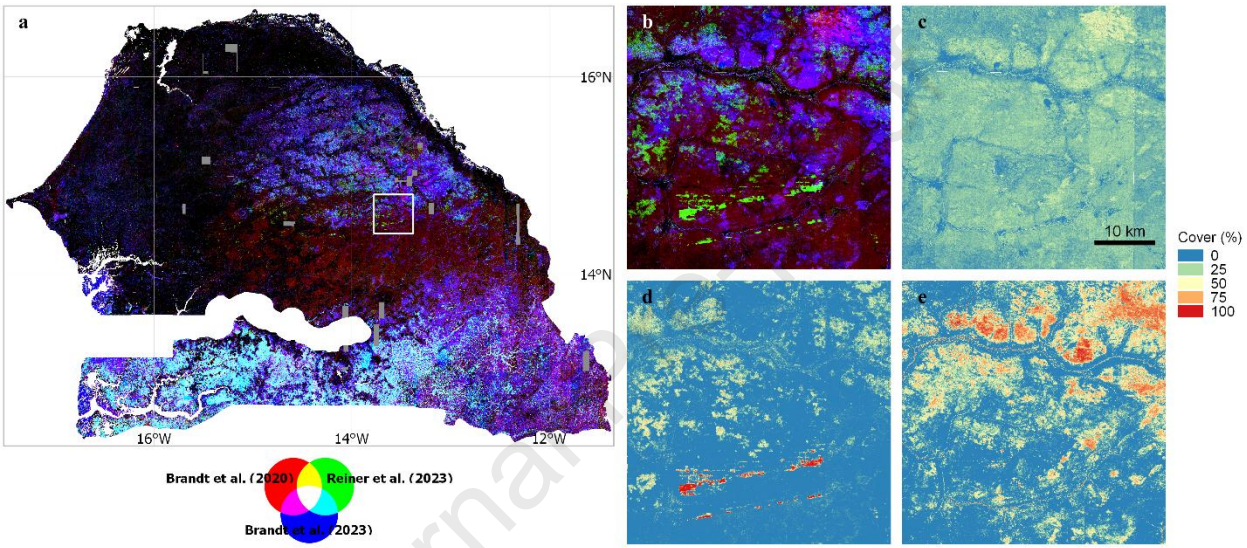


Fig. 4. The spatial disagreements among different maps. (a) The 30 m RGB composite cover map (red: Brandt et al. (2020); green: Reiner et al. (2023); blue: Brandt et al. (2023)) illustrating the spatial differences among different maps: the red, blue and green color indicates the notably high cover values of the corresponding map in comparisons to the other two; the cyan indicate the relative low values of Brandt et al. (2020); the magenta indicates the relative low values of Reiner et al. (2023) and yellow indicates the relative low values of Brandt et al. (2023) (not visually evident in this map). Gray rectangles indicate no-data areas in one or more of the maps. (b-e) A zoom-in example (extent marked in white rectangle in a) of the 30 m RGB composite, Brandt et al. (2020), Reiner et al. (2023) and Brandt et al. (2023), respectively.

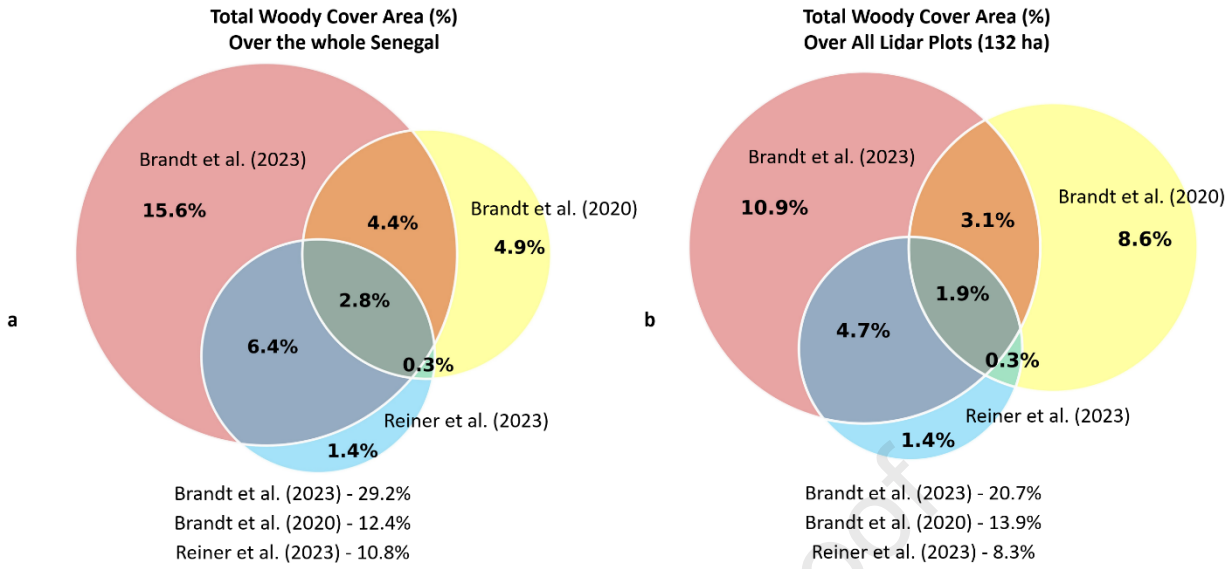


Fig. 5. Proportion of area mapped as tree/woody cover in one or more of the published tree cover maps (Brandt et al. (2020), Brandt et al. (2023) and Reiner et al. (2023)) over (a) the whole Senegal and (b) the UAV lidar flight area. The proportion was calculated as the target area (e.g., tree cover area in a specific map not overlapping with any other maps) divided by the total area of the UAV lidar plot/Senegal. The size of each section in the plot is proportional to the area it represents.

The result shows that each map differs in this best-matching structural definition: the Brandt et al. (2020) 0.5 m binary tree map best represents woody vegetation >4 m with >55% cover with a F-1 score of 0.235; the Reiner et al. (2023) 1 m binary tree map best represents woody vegetation >6 m with >53% cover with a F-1 score of 0.478; and the Brandt et al. (2023) 10 m tree probability map (binarized at ≥50% probability), represents woody vegetation >2 m with >34% cover with a F-1 score of 0.63 (Fig. 6; Table 2). However, the commission and omission errors vary greatly between the maps under these best matched height/cover definitions: Brandt et al. (2020) 0.5 m binary map yielded 23.4% producer's accuracy (PA) and 23.7% user's accuracy (UA). The low agreement is partly due to geolocation errors of the map, complicating submeter-level validation. This was supported by a plot-level georectification that doubled the original accuracy (PA = 50.1%, UA = 50%, F-1 score = 0.5) (S3). Beyond registration issues, an aggressive overestimation of tree crowns (Fig. 7, plot 9) and the limited ability to accurately depict continuous forest canopies (Fig. 7, plot 2) are main factors contributing to the low UA and PA. Reiner et al. (2023) 1 m binary map yielded 47.9% PA and 47.8% UA. Under the best matching definition, the map omits large parts of crown canopies over the north and middle Sudanian zone (Fig. 7, plot 5). Commission errors are widespread, including overestimates of dense vegetation (Fig. 7, plot 4). In the southern Sudanian area, the map has poor agreement with the lidar data, with both commission and omission errors common. The Brandt et al. (2023) 10 m map yielded 62.4% producer's accuracy and 63.1% user's accuracy. Overestimations include aggressive inclusion of scattered woody vegetation for agroforestry sites and northern Sahelian shrublands (Fig. 7, plot 20). Underestimation is evident in extensive areas of missed vegetation in the northeast Sudanian biome, which features continuous short woody cover with small unidentifiable crowns (Fig. 7, plot 6). The 35% probability threshold was not selected for the analysis, because the corresponding map-derived woody vegetation area (24.5%) exceeded even the lidar-derived area of vegetation >1 m, indicating substantial commission error for this threshold. Note that the accuracy curves in Fig. 6(b, c) are flat for Reiner et al. (2023) and Brandt et al. (2020). This is because in 1 m and

0.5 m resolutions, there are more pure pixels and fewer mixed pixels with intermediate values in the reference cover maps, leading to smaller differences in the area estimates when applying different cover thresholds (Fig. 3).

Table 2 Confusion matrix of each map vs. UAV lidar reference (ref) under the best matching height/cover definitions: (a) Brandt et al. (2020) (woody vegetation >4 m height, >55% cover). (b) Reiner et al. (2023) (woody vegetation >6 m height, >53% cover). (c) Brandt et al. (2023) (woody vegetation >2 m height, >34% cover). The first three columns represent the count of the reference pixels and map pixels. Please note that the confusion matrices represent pixel counts from an opportunistic sample. The values in brackets correspond to the standard errors.

a.

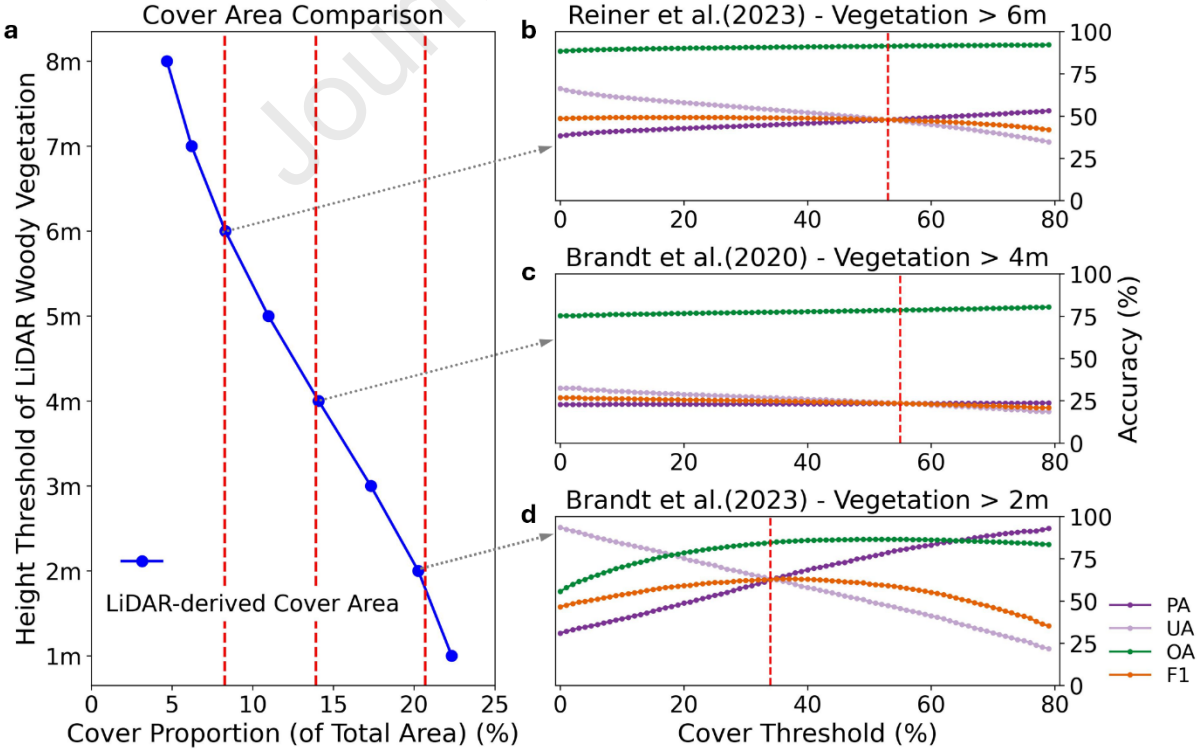
	Map - Yes	Map - No	PA	UA	OA	F1
Ref - Yes	210168	689458	23.4% (0.04%)	23.7% (0.05%)	78.6% (0.02%)	0.235
Ref - No	677419	4812633				

b.

	Map -Yes	Map - No	PA	UA	OA	F1
Ref - Yes	62130	67512	47.9% (0.14%)	47.8% (0.14%)	91.4% (0.02%)	0.478
Ref - No	67963	1383460				

c.

	Map - Yes	Map - No	PA	UA	OA	F1
Ref - Yes	1989	1199	62.4% (0.9%)	63.1% (0.9%)	84.5% (0.3%)	0.628
Ref - No	1161	10909				



Journal Pre-proof

Journal Pre-proof

Fig. 6. The best matching height/cover definitions for each map were identified through the area comparisons (a) and the binary accuracy assessment (b-d) using the UAV lidar data. (a) The area comparisons between the UAV lidar-derived woody vegetation cover area by different height definitions, and the three maps evaluated in this study: Brandt et al. (2020), Brandt et al. (2023) and Reiner et al. (2023). The lidar fly area totals 132 ha. The blue dot is the lidar-derived proportion of the total area covered by woody vegetation over the corresponding height threshold. Each red line represents the proportion of area covered by the mapped tree cover in the respective evaluated map from b-d. (b-d) The agreement of the maps (Reiner et al. (2023), Brandt et al. (2020) and Brandt et al. (2023)) with the UAV lidar-derived vegetation cover maps used as the reference. Brandt et al. (2023) was converted into a binary map using >=50% probability threshold for the purposes of comparison. For this assessment, the reference lidar data were converted into binary maps based on different height/cover thresholds (the height threshold obtained from (a) was used for each evaluated map, and varying cover thresholds demonstrated in (b-d)). The dotted red line represents cover thresholds in the reference data, with which the evaluated maps received the best balance of producer's accuracy (PA) and user's accuracy (UA). The confusion matrices corresponding to this height/cover threshold are provided in Table 2.

Journal Pre-proof

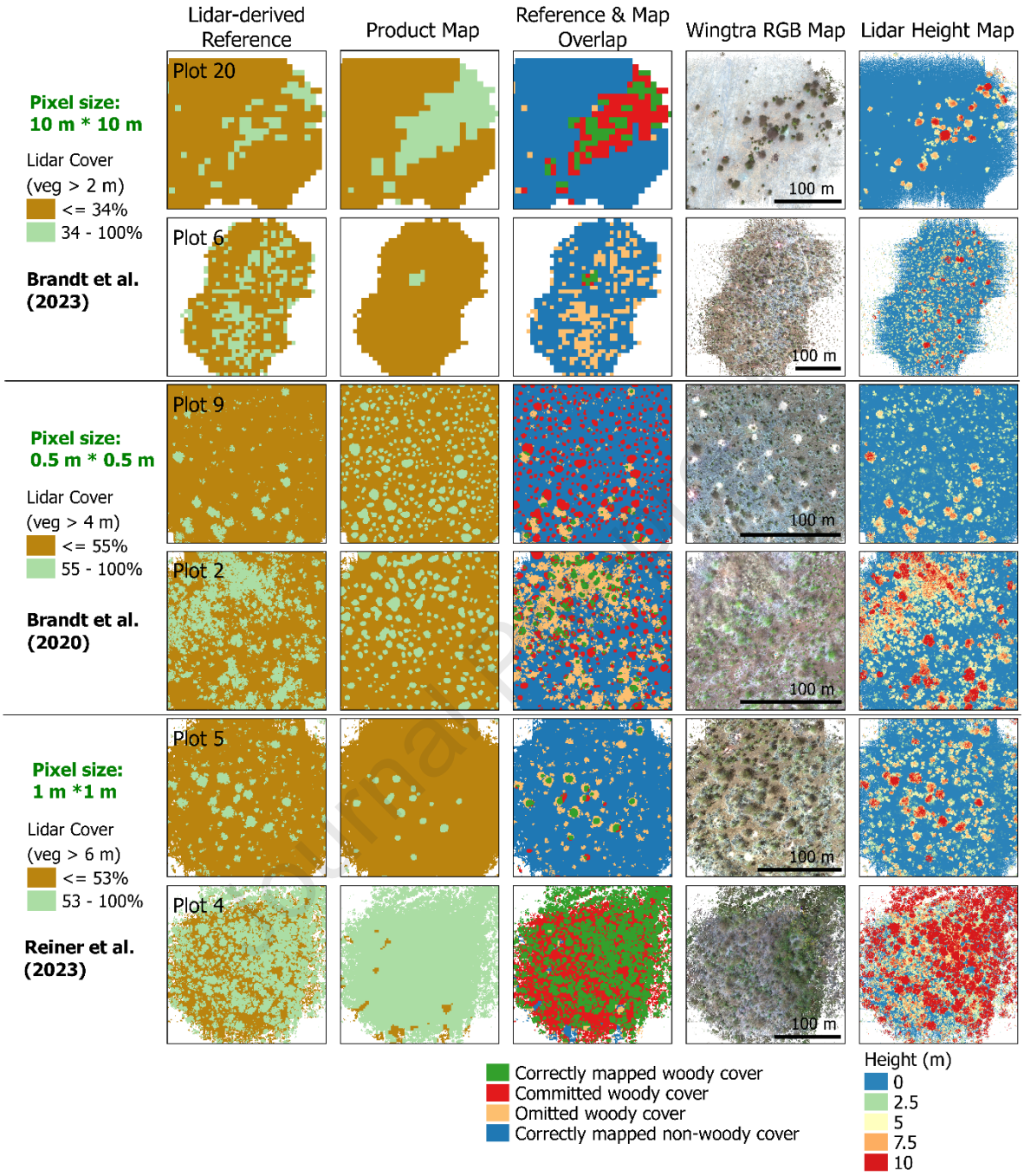


Fig. 7. Examples of issues in the maps of Brandt et al. (2023), Reiner et al. (2023) and Brandt et al. (2020). The first column is the reference UAV lidar-derived binary woody cover mask under the best-matching height/cover definition for the corresponding map. The second column is the published map (binary or converted to binary). The third column is the intersection of the UAV lidar and published map. The fourth column is the co-located UAV optical RGB imagery. The fifth column is the UAV lidar 10 cm max height image. The plot locations are shown in S1.

When overlapping the lidar binary reference under the most inclusive best-matching definitions (>2 m height, >34% cover) with all three maps over the lidar flight area, only 1.6% of the area has mapped tree/woody cover agreement from all four sources Fig. 8(a). Meanwhile, only half of the area mapped by Brandt et al. (2023) overlaps lidar woody cover, and for Brandt et al. (2020), less than 40%. When downscaling Brandt et al. (2020) and Reiner et al. (2023) and comparing all maps at a 10 m resolution, the results still show significant discrepancies with only 2.6% of the lidar flight area having mapped tree/woody cover agreements from all the sources Fig. 8(b), suggesting that differences in spatial resolution alone cannot explain the discrepancies. Although differences in temporal coverage may contribute to disagreements at the national scale (Fig. 4), temporal changes in woody cover cannot explain the discrepancies over the lidar reference areas, where pixels affected by such changes were excluded (Fig. 6-8). Note that though the sample of lidar sites is not probability-based, the cover estimate over lidar area is similar to that of country level, which indicates that the lidar sample is representative of the country (Fig. 5(b)).

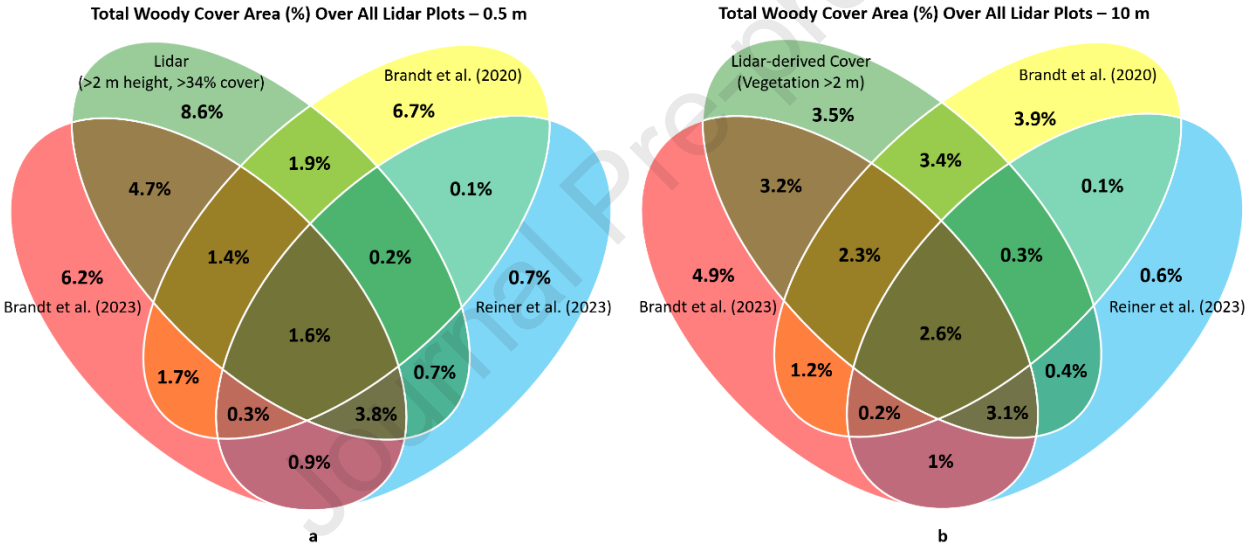


Fig. 8. (a) Proportion of the UAV lidar flight area with mapped tree/woody cover in the lidar-derived binary woody cover map and/or one or more of the published tree cover maps (Brandt et al. (2020), Brandt et al. (2023) and Reiner et al. (2023)) in 0.5 m scale. (b) Proportion of the UAV lidar flight area with mapped tree/woody cover in the lidar-derived woody cover map and/or one or more of the published tree cover maps (Brandt et al. (2020), Brandt et al. (2023) and Reiner et al. (2023)) in 10 m scale (When calculating, Reiner et al. (2023) 1 m and Brandt et al. (2020) 0.5 m binary maps were aggregated to the 10 m percent cover maps and the Brandt et al. (2023) 10 m probability value was used directly. We assumed that the mapped tree/woody cover in each pixel co-located among different sources). The proportion was calculated as the target area (e.g., tree cover area in a specific map not overlapping with any other maps or lidar reference data) divided by the total area of the UAV lidar plots.

6. Conclusion

The results of the map intercomparison highlight the pitfalls of dryland woody cover mapping. Peer-reviewed studies using higher spatial resolution imagery have extended our capabilities in quantifying this important global land cover. However, challenges of mapping dryland woody ecotones remain. Importantly, varying woody cover definitions preclude a consistent, convergent quantification of the extent

of dryland tree/shrub cover and a consensus understanding of this ecosystem. Very high spatial resolution data (e.g. DigitalGlobe) prove challenging given inconsistent acquisitions and resulting varying seasonality and sun-sensor-target geometry, and as shown here, inaccurate georeferencing that cannot be corrected systematically (S3(a)). Differences in sensor characteristics and their sensitivities to woody vegetation structure, algorithm type, and temporal coverage all contribute to inconsistencies among maps. Deep learning algorithms must be trained not only on individual trees across strictly defined height/cover thresholds, but also for continuous stands of varying height that do not present as discrete objects. In terms of monitoring, the challenge is even more pronounced, as mapping the woody cover dynamics requires accurate maps of the reference state. Consequently, any downstream applications that depend on these maps - such as biomass estimation, carbon accounting, ecosystem modeling or restoration efforts - are compromised.

We recommend that woody cover definitions return to the physiognomic-structural classifiers historically used by the UNFCCC and other international land monitoring initiatives. Like any theme of interest, there is a semantic limit to what meets the definition and what does not. Changing thematic definitions to fit an algorithm, for example using the diameter of a crown as the classifier, may limit the applicability of the resulting maps, as such definitions ignore the considerable extent of continuous and undifferentiated canopies with resulting impacts on land cover/land use, carbon, and habitat assessments. Definitions based on physiognomic-structural classifiers need to be consistently applied in mapping dryland ecotones. Increasingly available UAV/airborne lidar data are well-suited to the dryland woody cover mapping challenge, and large area studies should start with in-region lidar data as training, and more importantly, as validation, although these data typically have limited spatial and temporal coverage. Our lidar reference data were acquired during the dry season, and vegetation seasonality may affect the comparability between the lidar reference and the maps, emphasizing the importance of multi-season observations in future studies. Spaceborne lidar (e.g. GEDI and ICESat-2) provides large-scale vegetation structure information, but its use in dryland ecosystems is constrained by geolocation uncertainty and limited sensitivity to short woody vegetation (Hofton et al., 2019; Neuenschwander and Pitts, 2019). Advances in wall-to-wall spaceborne optical and radar observations (e.g. HLS, PlanetScope and NISAR) offer promising opportunities for improved large-scale woody cover characterization. In particular, the planned EDGE mission will provide the first areal scanning lidar from space and a possible resolution to the issues outlined here (Fricker et al., 2025). Together, a harmonized physiognomic-structural classification framework and advances in remote-sensing data availability will support consistent dryland woody cover characterization that enables comparable assessments of product quality and, ultimately, areal extent of woody cover, thereby providing a solid quantitative basis for dryland monitoring, and further applications.

Reference

Brandt, J., Ertel, J., Spore, J., Stolle, F., 2023. Wall-to-wall mapping of tree extent in the tropics with Sentinel-1 and Sentinel-2. *Remote Sensing of Environment* **292**, 113574. https://doi.org/10.1016/j.rse.2023.113574

Brandt, M., Rasmussen, K., Peñuelas, J., Tian, F., Schurgers, G., Verger, A., Mertz, O., Palmer, J.R.B., Fensholt, R., 2018. Reduction of tree cover in West African woodlands and promotion in semi-arid farmlands. *Nature Geoscience* **11**, 328–333. https://doi.org/10.1038/s41561-018-0092-x

Brandt, M., Tucker, C.J., Kariryaa, A., Rasmussen, K., Abel, C., Small, J., Chave, J., Rasmussen, L.V., Hiernaux, P., Diouf, A.A., Kergoat, L., Mertz, O., Igel, C., Gieseke, F., Schöning, J., Fensholt, R., 2020. An unexpectedly large count of trees in the West African Sahara and Sahel. *Nature* **587**, 78–82. https://doi.org/10.1038/s41586-020-2824-5

Brede, B., Lau, A., Bartholomeus, H.M., Kooistra, L., 2017. Comparing RIEGL RiCOPTER UAV LiDAR derived canopy height and DBH with terrestrial LiDAR. *Sensors* **17**, 2371. https://doi.org/10.3390/s17102371

DeFries, R.S., Townshend, J.R.G., 1994. NDVI-derived land cover classifications at a global scale. *International Journal of Remote Sensing* **15**, 3567–3586. https://doi.org/10.1080/01431169408954343

Di Gregorio, A., Leonardi, U., 2016. *Land Cover Classification System (LCCS) software version 3: User manual.* FAO, Rome, Italy.

Dinerstein, E., Olson, D., Joshi, A., Vynne, C., Burgess, N.D., Wikramanayake, E., Hahn, N., Palminteri, S., Hedao, P., Noss, R., Hansen, M., Locke, H., Ellis, E.C., Jones, B., Barber, C.V., Hayes, R., Kormos, C., Martin, V., Crist, E., Sechrest, W., Price, L., Baillie, J.E.M., Weeden, D., Suckling, K., Davis, C., Sizer, N., Moore, R., Thau, D., Birch, T., Potapov, P., Turubanova, S., Tyukavina, A., de Souza, N., Pintea, L., Brito, J.C., Llewellyn, O.A., Miller, A.G., Patzelt, A., Ghazanfar, S.A., Timberlake, J., Klöser, H., Shennan-Farpón, Y., Kindt, R., Barnekow Lillesø, J.-P., van Breugel, P., Graudal, L., Voge, M., Al-Shammari, K.F., Saleem, M., 2017. An ecoregion-based approach to protecting half the terrestrial realm. *BioScience* **67**(6), 534–545. https://doi.org/10.1093/biosci/bix014

FAO, 2023. *Terms and definitions—FRA 2025.* Food and Agriculture Organization of the United Nations, Rome.

Fricker, H.A., Armston, J.D., Blair, J.B., Luthcke, S.B., 2025. The Earth Dynamics Geodetic Explorer (EDGE) mission: A swath-imaging multifunction lidar for tracking the 3D structure of terrestrial ecosystems and surface topography of ice. *AGU Fall Meeting 2025*, New Orleans, Louisiana, 15–19 December 2025. [Poster presentation].

Hansen, M.C., DeFries, R.S., Townshend, J.R.G., Sohlberg, R., 2000. Global land cover classification at 1 km spatial resolution using a classification tree approach. *International Journal of Remote Sensing* **21**, 1331–1364. https://doi.org/10.1080/014311600210209

Hofton, M., Blair, J.B., Story, S., Yi, D., 2019. Algorithm Theoretical Basis Document (ATBD) for GEDI transmit and receive waveform processing for L1 and L2 products, version 1.0. NASA Goddard Space Flight Center, Greenbelt, MD.

IGBP, 1992. *Improved global data for land applications.* International Geosphere–Biosphere Programme, Stockholm.

ISO, 2023. *ISO 19144-2: Geographic information—Classification systems—Part 2: Land Cover Meta Language (LCML).* International Organization for Standardization, Geneva, Switzerland.

Küchler, A.W., 1949. A physiognomic classification of vegetation. *Annals of the Association of American Geographers* **39**, 201–210. https://doi.org/10.1080/00045604909352005

Journal Pre-proof

Loveland, T.R., Reed, B.C., Brown, J.F., Ohlen, D.O., Zhu, Z., Yang, L., Merchant, J.W., 2000. Development of a global land cover characteristics database and IGBP DISCover from 1 km AVHRR data. *International Journal of Remote Sensing* **21**, 1303–1330. https://doi.org/10.1080/014311600210191

Neuenschwander, A., Pitts, K., 2019. The ATL08 land and vegetation product for the ICESat-2 mission. *Remote Sens. Environ*. **221**, 247–259. https://doi.org/10.1016/j.rse.2018.11.005

Pan, Y., Birdsey, R.A., Fang, J., Houghton, R., Kauppi, P.E., Kurz, W.A., Phillips, O.L., Shvidenko, A., Lewis, S.L., Canadell, J.G., Ciais, P., Jackson, R.B., Pacala, S.W., McGuire, A.D., Piao, S., Rautiainen, A., Sitch, S., Hayes, D., 2011. A large and persistent carbon sink in the world's forests. *Science* **333**, 988–993. https://doi.org/10.1126/science.1201609

Pratt, D.J., Greenway, P.J., Gwynne, M.D., 1966. A classification of East African rangeland, with an appendix on terminology. *Journal of Applied Ecology* **3**, 369–382.

Reckziegel, R.B., Lowe, T., Devereux, T., Johnson, S.M., Rochelmeyer, E., Hutley, L.B., Doody, T., Levick, S.R., 2025. Assessing the reliability of woody vegetation structural characterisation from UAV-LS in a tropical savanna. *Science of Remote Sensing* **11**, 100178. https://doi.org/10.1016/j.srs.2024.100178

Reiner, F., Brandt, M., Kariryaa, A., Rasmussen, K., Mertz, O., Fensholt, R., 2023. More than one quarter of Africa's tree cover is found outside areas previously classified as forest. *Nature Communications* **14**, 2258. https://doi.org/10.1038/s41467-023-37877-8

Townshend, J.R.G., Justice, C.O., Li, W., Gurney, C., McManus, J., 1991. Global land cover classification by remote sensing: Present capabilities and future possibilities. *Remote Sensing of Environment* **35**, 243–255. https://doi.org/10.1016/0034-4257(91)90001-9

Tucker, C.J., 1979. Red and photographic infrared linear combinations for monitoring vegetation. *Remote Sensing of Environment* **8**, 127–150. https://doi.org/10.1016/0034-4257(79)90013-0

UNFCCC, 2001. *Land use, land-use change and forestry.* United Nations Framework Convention on Climate Change, Bonn, Germany.

Venter, Z.S., Cramer, M.D., Hawkins, H.-J., 2018. Drivers of woody plant encroachment over Africa. *Nature Communications* **9**, 2272. https://doi.org/10.1038/s41467-018-04616-8

White, F., 1983. *The vegetation of Africa: A descriptive memoir to accompany the UNESCO/AETFAT/UNSO vegetation map of Africa.* UNESCO, Paris. https://doi.org/10.5281/zenodo.293797

List of Figure Captions

Fig. 1. Example of woody cover classes as defined by height/cover thresholds. Bold arrows indicate skylight orthogonal to the ground that is intercepted by crown extent. Note that 'crown extent cover' here differs from the UAV lidar-derived foliar cover shown in Fig. 3, which refers to the leaf area intercepted by skylight. Figure adapted from Pratt et al. (1966).

Journal Pre-proof

Fig. 2. Ecoregions of Senegal and field study sites where UAV-based data were collected using RIEGL lidar equipment. Ecoregion boundaries are from Dinerstein et al. (2017). The change of the vegetation along the ecological gradient over the country is shown in the field photographs on the right.

Fig. 3. The workflow of converting UAV-derived 10cm max height maps to reference cover maps for different height thresholds (>1 m to >8 m) in different resolutions (0.5 m, 1 m, 10 m and 30 m). The calculations of single pixel cover for vegetation >2 m, >5 m and >8 m in 0.5 m are shown. Given that the within-crown gaps were accounted during calculation, the derived cover refers to foliar cover, which is the leaf area intercepted by vertical skylight.

Fig. 4. The spatial disagreements among different maps. (a) The 30 m RGB composite cover map (red: Brandt et al. (2020); green: Reiner et al. (2023); blue: Brandt et al. (2023)) illustrating the spatial differences among different maps: the red, blue and green color indicates the notably high cover values of the corresponding map in comparisons to the other two; the cyan indicate the relative low values of Brandt et al. (2020); the magenta indicates the relative low values of Reiner et al. (2023) and yellow indicates the relative low values of Brandt et al. (2023) (not visually evident in this map). Gray rectangles indicate no-data areas in one or more of the maps. (b-e) A zoom-in example (extent marked in white rectangle in a) of the 30 m RGB composite, Brandt et al. (2020), Reiner et al. (2023) and Brandt et al. (2023), respectively.

Fig. 5. Proportion of area mapped as tree/woody cover in one or more of the published tree cover maps (Brandt et al. (2020), Brandt et al. (2023) and Reiner et al. (2023)) over (a) the whole Senegal and (b) the UAV lidar flight area. The proportion was calculated as the target area (e.g., tree cover area in a specific map not overlapping with any other maps) divided by the total area of the UAV lidar plot/Senegal. The size of each section in the plot is proportional to the area it represents.

Fig. 6. The best matching height/cover definitions for each map were identified through the area comparisons (a) and the binary accuracy assessment (b-d) using the UAV lidar data. (a) The area comparisons between the UAV lidar-derived woody vegetation cover area by different height definitions, and the three maps evaluated in this study: Brandt et al. (2020), Brandt et al. (2023) and Reiner et al. (2023). The lidar fly area totals 132 ha. The blue dot is the lidar-derived proportion of the total area covered by woody vegetation over the corresponding height threshold. Each red line represents the proportion of area covered by the mapped tree cover in the respective evaluated map from b-d. (b-d) The agreement of the maps (Reiner et al. (2023), Brandt et al. (2020) and Brandt et al. (2023)) with the UAV lidar-derived vegetation cover maps used as the reference. Brandt et al. (2023) was converted into a binary map using >=50% probability threshold for the purposes of comparison. For this assessment, the reference lidar data were converted into binary maps based on different height/cover thresholds (the height threshold obtained from (a) was used for each evaluated map, and varying cover thresholds demonstrated in (b-d)). The dotted red line represents cover thresholds in the reference data, with which the evaluated maps received the best balance of producer's accuracy (PA) and user's accuracy (UA). The confusion matrices corresponding to this height/cover threshold are provided in Table 2.

Fig. 7. Examples of issues in the maps of Brandt et al. (2023), Reiner et al. (2023) and Brandt et al. (2020). The first column is the reference UAV lidar-derived binary woody cover mask under the best-matching height/cover definition for the corresponding map. The second column is the published map (binary or converted to binary). The third column is the intersection of the UAV lidar and published map.

The fourth column is the co-located UAV optical RGB imagery. The fifth column is the UAV lidar 10 cm max height image. The plot locations are shown in S1.

Fig. 8. (a) Proportion of the UAV lidar flight area with mapped tree/woody cover in the lidar-derived binary woody cover map and/or one or more of the published tree cover maps (Brandt et al. (2020), Brandt et al. (2023) and Reiner et al. (2023)) in 0.5 m scale. (b) Proportion of the UAV lidar flight area with mapped tree/woody cover in the lidar-derived woody cover map and/or one or more of the published tree cover maps (Brandt et al. (2020), Brandt et al. (2023) and Reiner et al. (2023)) in 10 m scale (When calculating, Reiner et al. (2023) 1 m and Brandt et al. (2020) 0.5 m binary maps were aggregated to the 10 m percent cover maps and the Brandt et al. (2023) 10 m probability value was used directly. We assumed that the mapped tree/woody cover in each pixel co-located among different sources). The proportion was calculated as the target area (e.g., tree cover area in a specific map not overlapping with any other maps or lidar reference data) divided by the total area of the UAV lidar plots.

S1. The images and locations of all the UAV lidar plots. The first column shows the 10 cm gridded max height of all the lidar plots. The second column shows the Wingtra UAV RGB optical image of the plots, which was taken at the same time with lidar data collection.

S2 The comparison between Brandt et al. (2023) 10 m tree extent probability and lidar-derived 10 m woody vegetation cover. The lidar-derived cover adopted here was under the best-matching woody vegetation height definition (>2 m) of Brandt et al. (2023) (Fig. 6).

S3. The geolocation of Brandt et al. (2020) were calibrated using the lidar data over each plot and the resulting calibrated data were compared to the lidar binary reference data. **a,** the per-plot shifts of Brandt et al. (2020) along x and y during geolocation calibration; **b,** an example (plot 22, S1) showing the differences between the before-calibration and after-calibration Brandt et al. (2020) data; **c,** the accuracy of the calibrated Brandt et al. (2020) with the UAV lidar-derived vegetation cover maps used as the reference. The reference data are converted into binary maps based on different cover thresholds (the height threshold obtained from Extended Fig. 3a was used). The dotted red line represents cover threshold in the reference data, with which the evaluated maps received the best balance of producer's accuracy (PA) and user's accuracy (UA); and **d,** Confusion matrix of Brandt et al. (2020) (map) vs. UAV lidar reference (ref) under the best matching height/cover definitions (woody vegetation >4 m height, 40% cover). The values in brackets correspond to the standard errors.

Acknowledgements

The work is funded by Bezos Earth Fund Land and Carbon Lab (G2436). We thank Centre de Suivi Ecologique for their support in our field data collection.

Author Contributions

X.L. and M.H. conceptualized and designed the study. X.L., M.H., C.M., A.M.D., A.A.D., A.H., J.P., B.N., C.M.M.M. and K.M. contributed to field data collections. X.L., M.H., P.P., A.T. and A.P. prepared the code and sources for data processing and analysis. X.L. and M.H. conducted the analysis. X.L., M.H., P.P. and A.T. drafted the manuscripts and C.M., A.A.D. and A.H. contributed to further editing and revising.

554 **Competing Interests**

555 The authors declare no competing interests.

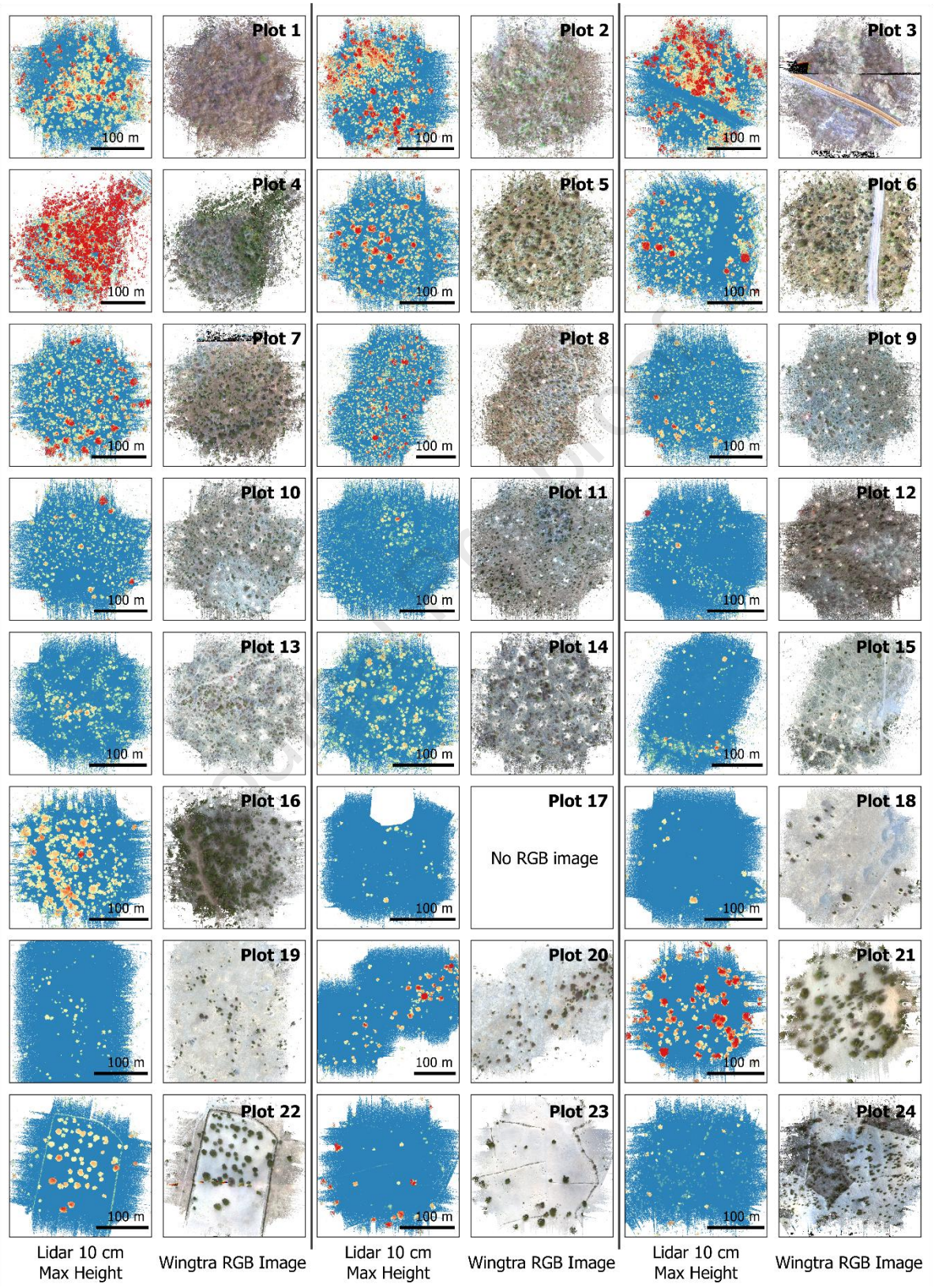
556 **Data Availability**

557 The TIFF data of the lidar flights will be available by sending email to the corresponding author upon
558 reasonable request. The individual tree canopy map from Brandt et al. (2020) is available at the Oak Ridge
559 National Laboratory at https://doi.org/10.3334/ORNLDAAC/1832. The tree extent map from Brandt et al.
560 (2023) is available at https://datasets.wri.org/. The tree cover map from Reiner et al. (2023) is available at
561 100 m resolution at https://doi.org/10.5281/zenodo.7764460, and is available at 1 m upon request.

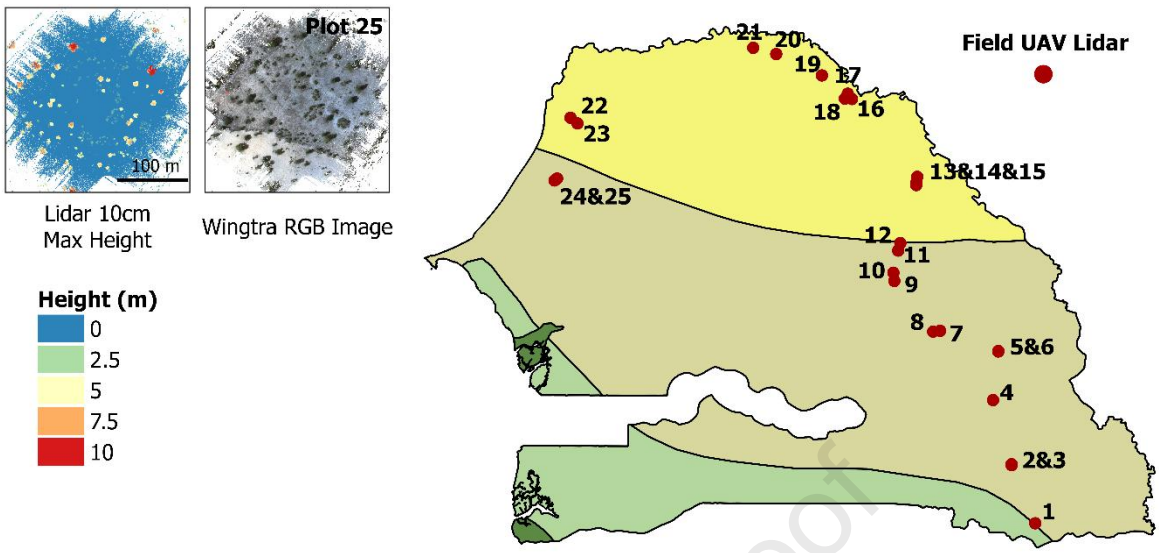
562

Journal Pre-proof

563 **Supplementary Information**

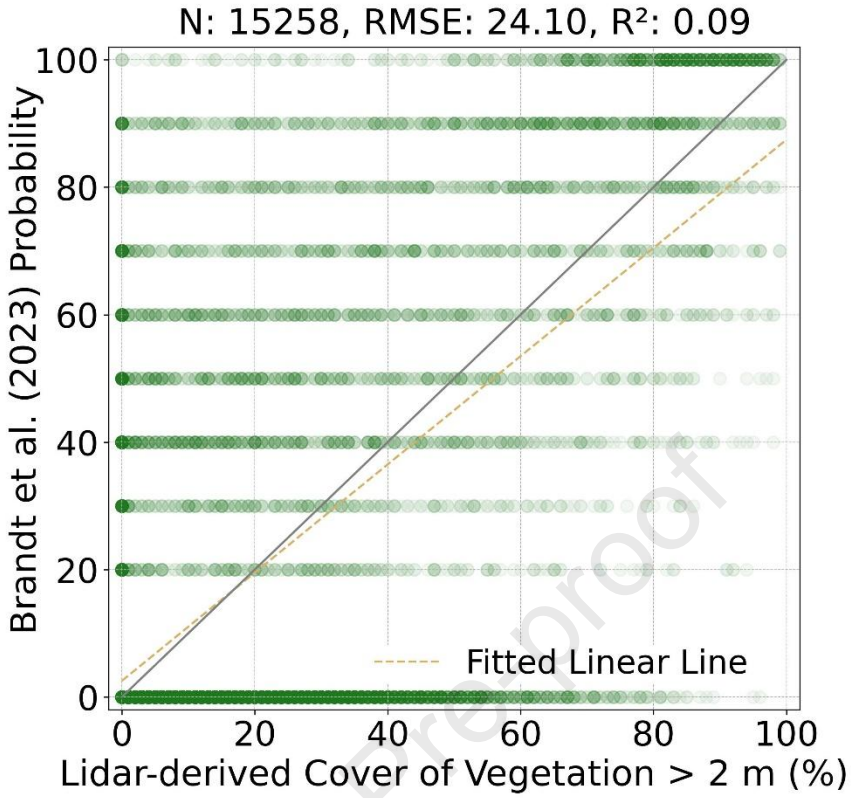


564



S1. The images and locations of all the UAV lidar plots. The first column shows the 10 cm gridded max height of all the lidar plots. The second column shows the Wingtra UAV RGB optical image of the plots, which was taken at the same time with lidar data collection.

Journal Pre-proof

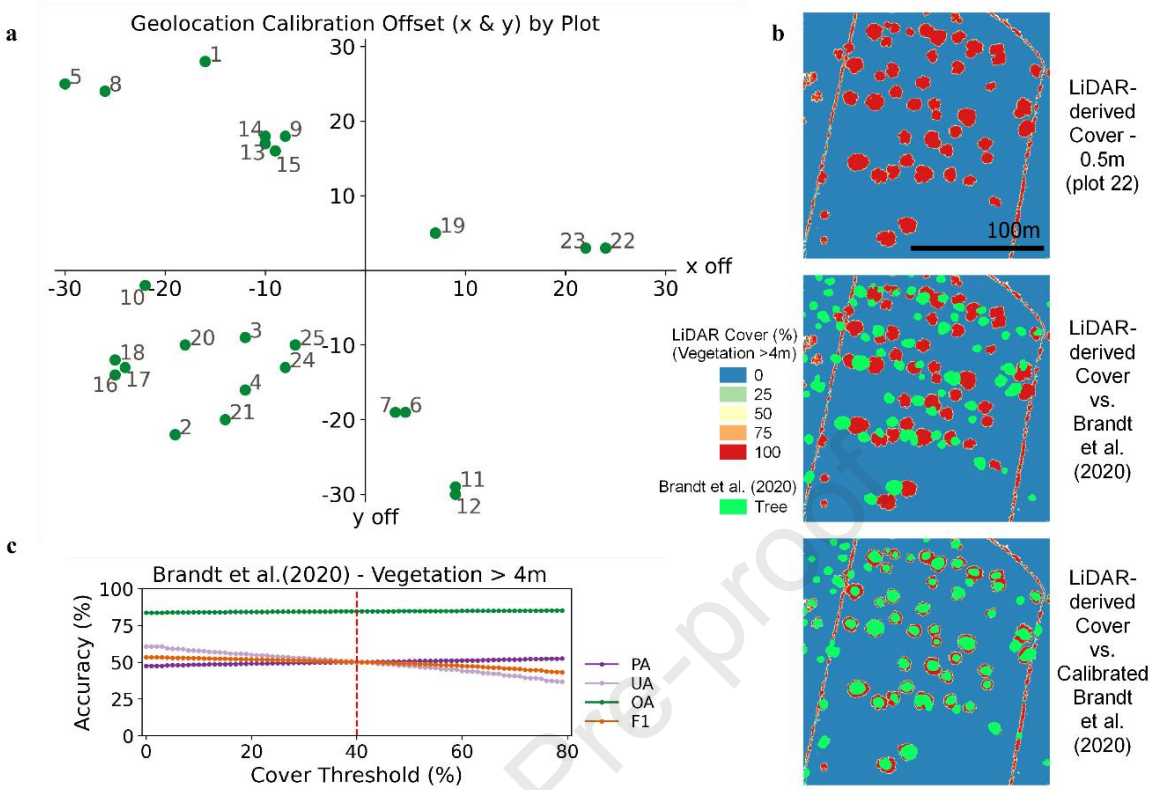


595

596 **S2** The comparison between Brandt et al. (2023) 10 m tree extent probability and lidar-derived 10 m woody
597 vegetation cover. The lidar-derived cover adopted here was under the best-matching woody vegetation
598 height definition (>2 m) of Brandt et al. (2023) (Fig. 6).

599

Journal Pre-proof



600
601 **d.**

	Map - Yes	Map - No	PA	UA	OA	F1
Ref - Yes	494424	492240	50.1% (0.05%)	50.0% (0.05%)	84.6% (0.01%)	0.50
Ref - No	494847	4908168				

602 **S3.** The geolocation of Brandt et al. (2020) were calibrated using the lidar data over each plot and the
603 resulting calibrated data were compared to the lidar binary reference data. **a,** the per-plot shifts of Brandt et
604 al. (2020) along x and y during geolocation calibration; **b,** an example (plot 22, S1) showing the differences
605 between the before-calibration and after-calibration Brandt et al. (2020) data; **c,** the accuracy of the
606 calibrated Brandt et al. (2020) with the UAV lidar-derived vegetation cover maps used as the reference.
607 The reference data are converted into binary maps based on different cover thresholds (the height threshold
608 obtained from Extended Fig. 3a was used). The dotted red line represents cover threshold in the reference
609 data, with which the evaluated maps received the best balance of producer's accuracy (PA) and user's
610 accuracy (UA); and **d,** Confusion matrix of Brandt et al. (2020) (map) vs. UAV lidar reference (ref) under
611 the best matching height/cover definitions (woody vegetation >4 m height, 40% cover). The values in
612 brackets correspond to the standard errors.
613

614

Journal Pre-proof

- Three advanced woody cover maps show low spatial agreement across Senegal
- Only 2.8% of Senegal has woody cover identified by all three maps
- UAV lidar shows maps correspond to different physiognomic-structural thresholds
- Harmonized physiognomic-structural definitions are needed for dryland mapping

Journal Pre-proof

Journal Pre-proof

Declaration of interests

☒ The authors declare that they have no known competing financial interests or personal relationships that could have appeared to influence the work reported in this paper.

☐ The authors declare the following financial interests/personal relationships which may be considered as potential competing interests:

Journal Pre-proof